Dicoordinate Au(I)–Ethylene Complexes as Hydroamination Catalysts

Miquel Navarro*, Macarena G. Alférez, Morgane de Sousa, Juan Miranda-Pizarro, Jesús Campos*

[†] Instituto de Investigaciones Químicas (IIQ), Departamento de Química Inorgánica and Centro de Innovación en Química Avanzada (ORFEO−CINQA). Consejo Superior de Investigaciones Científicas (CSIC) and University of Sevilla, 41092 Sevilla, Spain

E-mail: miquel.navarro@iiq.csic.es; jesus.campos@iiq.csic.es

Abstract

A series of gold(I)–ethylene π complexes containing a family of bulky phosphine ligands has been prepared. The use of these sterically congested ligands is crucial to stabilize the gold(I)–ethylene bond and prevent decomposition, boosting up their catalytic performance in the highly underexplored hydroamination of ethylene. The precatalysts bearing the most sterically demanding phosphines showed excellent results reaching full conversion to the hydroaminated products under low ethylene pressure (1 bar). Kinetic analysis together with density functional theory (DFT) calculations revealed that the assistance of a second molecule of the nucleophile as a proton shuttle is preferred even when using an extremely congested cavity-shaped Au(I) complex.

Introduction

For decades gold was considered too chemically inert to be used in catalysis.[1] However, since the discovery of its ability to activate π-bonds towards nucleophilic addition, molecular gold complexes have played a prominent role in the catalytic transformation of unsaturated hydrocarbons.[2] The number of reactions mediated by π-acid gold catalysis is extensive and includes hydrogenation, oxidation, diarylation, heteroarylation or cycloadditions, among many others.[3] A type of transformation that has been extensively studied as a versatile route to prepare nitrogen-containing compounds with optimal atom economy is hydroamination, that is, the addition of an N–H unit of nucleophilic amines (or related substrates) across a carbon–carbon multiple bond.[4] Although these processes can be mediated by other transition metals[5] and even through metal-free protocols,[6] gold(I) complexes remain as one of the most powerful hydroamination catalysts.[3j,7] In fact, they can accomplish the intermolecular hydroamination of C≡C triple bonds[8] and even the more challenging C=C double bonds,[9,10] in some cases even for inactivated alkenes.[11] For the latter, the Au(I)-catalyzed hydroamination of ethylene, the simplest alkene, has only been reported once.[12]

Coordination of a C–C multiple bond to form a gold π-complex is usually proposed as the initial step during π-acid catalyzed reactions, including hydroamination. Thus, the isolation of gold π-complexes has gathered considerable interest associated to their catalytic relevance, since they serve as models for the transient gold π-complexes.[13] Among those, cationic dicoordinate gold(I) π-complexes of substituted alkenes and alkynes have been isolated and characterized over the last decade using phosphine or N-heterocyclic carbene (NHC) ligands.[14] Chelating N- and P-based ligands have also proved useful to form tricoordinate gold π-complexes.[15] However, despite the interest on developing efficient methods for ethylene functionalization, gold(I)–ethylene complexes are quite rare.[16,17] In fact, we have recently authenticated the first dicoordinate gold(I)–ethylene adduct by using the extremely bulky tris-2-(4,4'-di-*tert*-butylbiphenylyl)phosphine (**L1**), previously reported by Straub,[18] that kinetically stabilizes the coordination of ethylene.[19] In contrast to related tricoordinate complexes, the bonding interactions are mainly electrostatic (i.e. ionic) with minimal Au→ethylene π-backdonation.

This strategy of using sterically demanding ligands to detect and isolate transient intermediates of relevance to catalytic processes have proved successful in the past. Our group has also committed to the task, capitalizing on the steric shrouding provided by terphenyl (C_6H_3-2,6-Ar_2) phosphine ligands.[20] For instance, these have been used to access unusual gold compounds, such as the first methyl-bridged cationic digold complexes[21] and to study their relevance in C–C coupling processes,[22] as well as to exploit gold species as frustrated Lewis pair (FLP) constituents.[23] In this study, we have selected a family of bulky phosphine ligands in an attempt

to access rare Au(I)-ethylene adducts. More precisely, we have used both the commercial ligands trimesityl phosphine (**L2**) and tBuXPhos (**L3**), as well as a series of terphenyl phosphines (**L4–L8**) prepared in our group (Figure 1).[24] We compare herein the stability of the resulting ethylene adducts with respect to the first of its class constructed around **L1**[19] and examine their catalytic competence for the underdeveloped Au(I)-catalyzed functionalization of ethylene through a model hydroamination reaction.
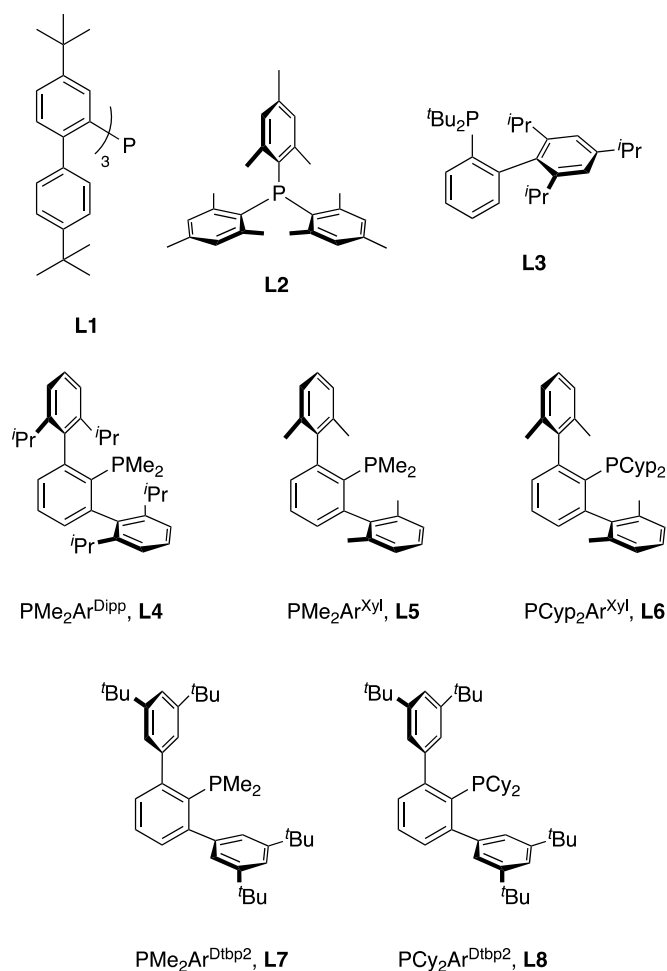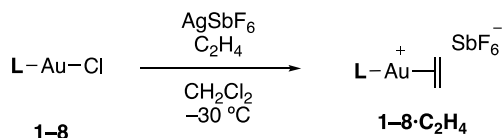

Figure 1. Selected bulky phosphine ligands used in this study.

Results and discussion

Synthesis of gold(I)–ethylene complexes. The reaction of [AuCl(THT)] (THT = tetrahydrothiophene) with phosphine ligands **L1–L8** in dichloromethane forms the air-stable, neutral phosphine chloride complexes **1–8**. The steric bulkiness of the phosphine ligands was evaluated calculating the percent buried volume (%V_{bur}),[25] which yielded notably large parameters (Table 1 and Figure S63). Nonetheless, there are clear differences in the steric shrouding imparted by the employed phosphines. Terphenyl phosphine ligands containing two

small methyl groups bound to the phosphorus atom present lower $\%V_{bur}$ values, ranging from 38.2 in **L5** to 46.2 in **L4** after substituting the methyl groups on the flanking aryl rings of the terphenyl substituent by isopropyl termini. Similar $\%V_{bur}$ parameters were measured for **L7** and the widely used trimesityl phosphine (**L2**). Introducing bulkier substituents bound to the phosphorus atom in **L6** and **L8** increased the $\%V_{bur}$ to around 53, comparable to the Buchwald-type phosphine **L3**. Albeit the former are considerably bulky, the tris biaryl tris-2-(4,4'-di-*tert*-butylbiphenylyl)phosphine phosphine (**L1**) clearly presents the highest $\%V_{bur}$ value of 67.0.[19] As discussed in the following sections, the steric profile of the ligand seems to be crucial to impart stability to the aimed Au(I)-ethylene compounds, having a direct effect on catalytic performance.

Treatment of gold(I) chloride complexes **1–8** with $AgSbF_6$ under an ethylene atmosphere at –30 °C caused instantaneous precipitation of AgCl and formation of the gold(I)–ethylene complexes **1–8·C₂H₄** (Scheme 1). Filtration of aforementioned reaction mixtures through short pads of Celite followed by washing with pentane afforded the pure gold(I) π-complexes **1–8·C₂H₄** in good to excellent yields (53–93%). The reactions were conveniently monitored by $^{31}P\{^{1}H\}$ NMR spectroscopy, which revealed a systematic downfield shift in the range from 4.3 to 10.0 ppm compared to the corresponding gold(I) chloride complexes (Table 1). It is worth noting that attempts to prepare the related $[(Ph_3P)Au(C_2H_4)]^+$ complex led to immediate decomposition and formation of $[(PPh_3)_2Au]^+$ and Au(0), likely due to the inability of the relatively small PPh_3 ligand to kinetically stabilize the corresponding Au(I)-ethylene adduct.

Scheme 1. Synthesis of gold(I)–ethylene complexes **1–8·C₂H₄** (L = **L1**–**L8** from Figure 1).

Complexes **2–8·C₂H₄** were spectroscopically characterized in dichloromethane solution under ethylene atmosphere to prevent decomposition, which accelerates upon removal of the gaseous substrate. In some cases and due to the chemical exchange between coordinated and free ethylene (*vide infra*), the two signals were undistinguishable. To unambiguously identify the resonances belonging to coordinated ethylene, ^{1}H and $^{13}C\{^{1}H\}$ NMR spectroscopy were also performed in absence of ethylene, though in those cases signs of decomposition were evident by NMR spectroscopy (see SI for more details). Nonetheless, these studies permitted the unambiguous assignment of the targeted ethylene adducts; resonances associated to the coordinated olefin were found to differ from those of the free molecule (Table 1). Thus, coordination to gold(I) induces a noticeable upfield shift of the ^{1}H NMR signals (~0.5 ppm) with the exception of complex **2·C₂H₄**, which is only slightly downfield shifted by 0.06 ppm. In turn, $^{13}C\{^{1}H\}$ NMR resonances are

shifted in the same direction with upfield shifts about 7 ppm with respect to free ethylene (Table 1). These relatively small changes suggest little backdonation from Au to the ethylene $\pi^*(C=C)$ orbital, as noted earlier for **1·C₂H₄**,[19] and in contrast with the related tricoordinate gold(I)–ethylene complexes,[13f] in which the chemical shift differences can reach up to 3 ppm and 55 ppm in ^{1}H and ^{13}C NMR spectra, respectively. As for the more sterically hindered complex **1·C₂H₄**,[19] the coordinated ethylene presented the largest shift in ^{1}H NMR resonances, which appear as an AA'BB' system at 3.79 and 3.66 ppm, contrasting with the rest of compounds that led to a single broad peak due to four equivalent protons. We ascribed the shift in **1·C₂H₄** to ring-current effects due the surrounding aryl rings, which could also hinder the rotation of bound ethylene giving rise to the observed AA'BB' system. Chemical exchange between coordinated and free ethylene was observed in CD_2Cl_2 within the NMR timescale for all ethylene adducts, however, its rate could not be reliably quantified due to the rapid exchange and close proximity of the respective NMR signals, which prevented accurate data analysis.

Table 1. Selected spectroscopic and structural data of complexes **1–8·C₂H₄**.

Compound	δ^{1}H (ppm)	δ^{13}C (ppm)	δ^{13}P (ppm)^a	%V$_{bur}$^{b}	d(C=C) (Å)
ethylene^c	5.43	116.8	-	-	1.313
1·C₂H₄^d	3.66; 3.79	110.2	13.1(9.5)	67.0	1.236(10)
2·C₂H₄	5.46	111.2	1.5(–5.4)	45.3	-
3·C₂H₄	4.95	110.9	65.6(58.6)	55.5	1.353(15)
4·C₂H₄	4.85	110.3	4.3(–5.7)	46.2	-
5·C₂H₄	5.00	111.5	4.1(–3.2)	38.2	-
6·C₂H₄	4.86	111.0	57.6(53.3)	53.5	-
7·C₂H₄	5.16	111.8	9.3(0.4)	45.0	-
8·C₂H₄	4.77	109.0	55.4(48.8)	53.7	1.384(10)

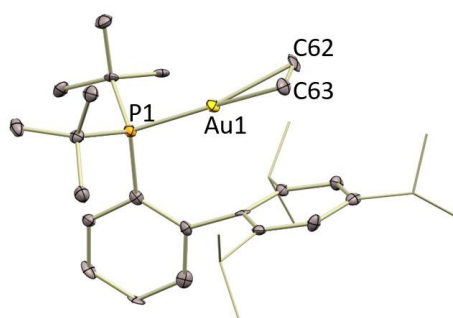^{a}The corresponding δ ^{31}P NMR of the gold chloride complexes **1–8** is indicated in parentheses. ^{b}%V$_{bur}$ is calculated from the corresponding gold(I) chloride complexes **1–8** (see SI). ^{c}Data from ref. 26. ^{d}Data from ref. 19.

Single crystals of complexes **3·C₂H₄** and **8·C₂H₄** suitable for X-ray diffraction analysis were obtained by slow diffusion of pentane into saturated dichloromethane solutions of the gold(I) ethylene complexes at –30 °C. Both species adopt similar structures in the solid state, with the gold center in a linear environment and the ethylene molecule coordinated in a η^2-fashion (Figure 2). It is worth noting that in contrast to complexes **1·C₂H₄** and **3·C₂H₄**, the coordination of
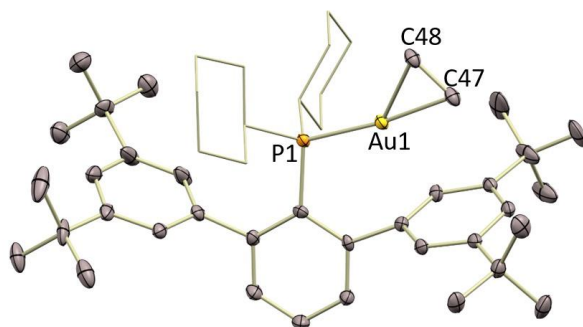
ethylene to gold in $8 \cdot \mathbf{C_2H_4}$ is highly dissymmetric: the ethylene molecule is notably slipped, that is, whereas it presents similar Au–C bond distances, the P–Au–C angles of 173.55(19)° and 137.2(2)° are remarkably different. In complexes $3 \cdot \mathbf{C_2H_4}$ and $8 \cdot \mathbf{C_2H_4}$ the Au–C bond lengths (2.21–2.26Å) are noticeably longer than those described for gold(I)–ethylene adducts bearing bidentate ligands (*ca.* 2.14–2.17 Å),[15,16] but similar to $1 \cdot \mathbf{C_2H_4}$ (2.216(6) and 2.235(6) Å) and related cationic dicoordinate gold(I) π-complexes of other alkenes.[14] The C=C double bond ($3 \cdot \mathbf{C_2H_4}$, 1.353(15) Å; $8 \cdot \mathbf{C_2H_4}$, 1.384(10) Å) is slightly longer than that of free ethylene (1.313 Å)[26] and complex $1 \cdot \mathbf{C_2H_4}$ (1.263(10) Å) and similar to those described for tricoordinate gold(I) ethylene compounds,[16] despite the expected poor Au→ethylene π-backdonation.

It was mentioned above that gold(I)–ethylene complexes 2–$8 \cdot \mathbf{C_2H_4}$ exhibit slow decomposition both in solid state and in dichloromethane solution upon removal of the ethylene atmosphere, which contrasts with the remarkable stability of $1 \cdot \mathbf{C_2H_4}$ that we have attributed to the kinetic stabilization imparted by the cavity-shaped phosphine. For all other cases monitoring the evolution of dichloromethane solutions of the ethylene adducts by $^{31}P\{^1H\}$ NMR spectroscopy revealed the presence of the corresponding $[P–Au–P]^+$ decomposition products along with Au(0) nanoparticles as the major products.[22,27,28] Nonetheless, the appearance of other broad $^{31}P\{^1H\}$ signals evince the formation of additional species. For instance, after a few days in solution the decomposition spectrum of complex $6 \cdot \mathbf{C_2H_4}$ revealed the formation of a relatively broad $^{31}P\{^1H\}$ NMR signal at 50.3 ppm distinct to the one corresponding to $[(PCyp_2Ar^{Xyl2})_2 –Au]^+$ (53.4 ppm). X-ray diffraction studies allowed us to ascertain the formation of a new gold(I) cationic species ($[6]_\omega$) with a highly unusual polymeric structure derived from ethylene release and subsequent η^2-coordination of a side aryl ring of the terphenyl substituent of an adjacent cationic gold fragment (Figure 2). The η^2-coordination of the xylyl ring is slightly slipped with different Au–C distances of 2.301(6) Å and 2.401(7) Å, and notably different P–Au–C angles of 169.2(2)° and 151.5(2)°, respectively. This structure is reminiscent of π-arene complexes of gold formed in aromatic solvents, which have been reported in several occasions and whose geometric parameters are comparable to $[6]_\omega$.[29] However, this seems to be the first polymeric structure of this kind in which the building blocks are solely units of $[LAu]^+$ connected by π-coordination.

Attempts to prepare other polymeric structures of this type by direct treatment of compounds 1–8 with equimolar amounts of AgSbF$_6$ in dichloromethane were unsuccessful. In fact, while under ethylene atmosphere instant precipitation of AgCl upon addition of the silver reagent was visually identified, this did not occur in the absence of the olefin, arguing in favor of the presence of silver within the resulting structure. This was not surprising considering our previous report on the reaction of complex 1 and AgSbF$_6$, which resulted in the formation of a gold–silver trimetallic species without chloride abstraction. In the case of compounds 2 and $[(Ph_3P)AuCl]$, generation of the corresponding homoleptic $[P–Au–P]^+$ complexes and Au(0) nanoparticles was exclusively
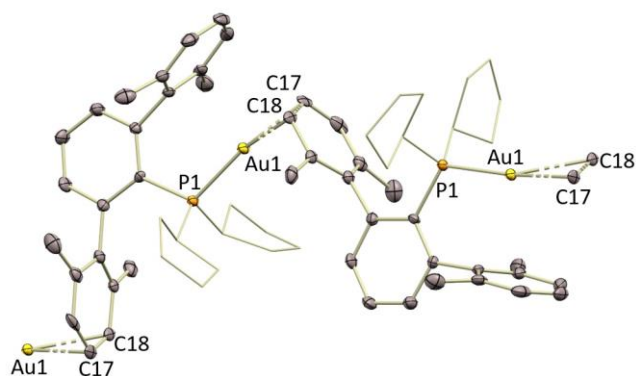
observed. In contrast, complexes **3**–**8** bearing bulky biphenyl and terphenyl phosphine ligands do not lead to their corresponding [P–Au–P]$^+$ complexes, but form instead other species characterized by broad NMR resonances that we tentatively attribute to gold(I)–silver(I) multimetallic complexes by analogy with our prior studies on compound **1**. This notion is further supported by diffusion-ordered NMR experiments. For instance, ^{1}H DOSY experimental data revealed a diffusion coefficient for the in situ equimolar reaction between complex **6** and AgSbF$_6$ (D) equal to $9.13 \cdot 10^{-10}$ m/s^2, that accounts for only half of that for pure **6·C$_2$H$_4$** (D = $1.75 \cdot 10^{-9}$ m^2/s), (See SI for more details), indicating a larger structure attributable to a multimetallic species in the former case.
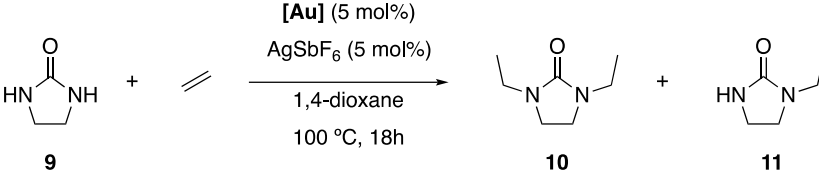

3·C$_2$H$_4$

8·C$_2$H$_4$

[6]$_\infty$

Figure 2. ORTEPs of complexes **3·C$_2$H$_4$**, **8·C$_2$H$_4$** and **[6]$_\infty$**. Thermal ellipsoids are set at 50% probability. Selected bond lengths (Å) and angles (°): compound **3·C$_2$H$_4$**, (one of two independent molecules per asymmetric unit; selected parameters from the one not showing disorder in the ethylene ligand), P1–Au1, 2.289(2); Au1–C62, 2.237(9); Au1–C63, 2.261(9); C62–C63, 1,353(15); P1–Au1–C62, 149.2(3); P1–Au1–C63, 164.8(3); compound **8·C$_2$H$_4$**, P1–Au1, 2.2977(16); Au1–C47, 2.210(7); Au1–C48, 2.227(7); C47–C48, 1.384(10); P1–Au1–C47, 173.54(19); P1–Au1–C48, 137.2(2); compound **[6]$_\infty$**, P1–Au1, 2.2633(15); Au1–C17, 2.301(6); Au1–C18, 2.403(6); C17–C18, 1.385(11); P1–Au1–C17, 169.2(2); P1–Au1–C18, 151.5(2).

Catalytic hydroamination of ethylene. Having on hand the first examples of stable dicoordinate Au(I)-ethylene compounds we next examined their catalytic potential in the hydroamination of the coordinated olefin. Initially, imidazolidine-2-one (**9**)[12] was used as a model substrate to gauge the activity of all cationic gold(I)-ethylene species, obtained in situ from its corresponding neutral chloride precursors. Thus, solutions of compound **9** were pressurized with ethylene (4 bar) in the presence of 5 mol% of the gold(I) chloride **1**–**8** complex and 5 mol% of AgSbF$_6$ as halide scavenger in dioxane at 100 °C. Complexes **1**, **3**, **6** and **8** displayed great catalytic activity, reaching full conversion to the double hydroamination product 1,3-ethylimidazolidin-2-one (**10**) after 18 h (Table 2, entries 1, 4, 7 and 9), while formation of the monohydroaminated species was not detected. Interestingly, these complexes bear the bulkier phosphine ligands, with %V$_{bur}$ values between 53.5 and 67.0. On the contrary, low or no conversion was obtained when employing complexes **2**, **4**, **5**, **7** and [PPh$_3$AuCl] (Table 2, entries 3, 5, 6, 8 and 10), which present smaller phosphine ligands with %V$_{bur}$ below 46.2.

^{31}P{^{1}H} NMR spectroscopy analysis of the final catalytic mixtures after 18 h revealed the presence of the independently authenticated gold(I)–ethylene complexes in most cases, together with variable amounts of the corresponding free phosphine ligands. However, in the case of complexes **2**, **4**, **5** and [(Ph$_3$P)AuCl], the corresponding [P–Au–P]$^+$ complexes were clearly observed as the major or sole gold-containing species. Formation of the latter under catalytic conditions is in agreement with our prior stability studies, and can be understood as a deactivation pathway for the gold(I) complexes bearing the smaller phosphine ligands (Scheme 2), while more hindered phosphines prevent or slow down this unproductive route. Control experiments were also performed in order to investigate whether the presence of silver ions could have a direct influence on the catalytic outcome, as previously reported in other gold-catalyzed processes[30]. No conversion was observed in the absence of gold(I) complex (Table 2, entry 11) nor in the presence of a combination of 5 mol% of **L1** or **L2** and AgSbF$_6$ (Table 2, entries 12 and 13), indicating that under these conditions silver(I) is not capable of catalyzing the hydroamination of ethylene. In addition, the solvento complex **1·MeCN**[19] was used in the absence of AgSbF$_6$ achieving full conversion after 18 h, ruling-out a direct silver-effect during gold catalysis (Table 2, entry 2).[30]

Table 2. Gold(I)-catalyzed hydroamination of ethylene by imidazolidine-2-one.[a]

entry	Catalyst	$P_{ethylene}$ (bar)	Conversion %[b]	**10:11**
1	**1**	4	>99	100:0
2	**1·MeCN**[c]	4	>99	100:0
3	**2**	4	0	-
4	**3**	4	>99	100:0
5	**4**	4	<5	n.d.[d]
6	**5**	4	<5	n.d.[d]
7	**6**	4	95	100:0
8	**7**	4	20	15:85
9	**8**	4	>99	100:0
10	[(Ph₃P)AuCl]	4	0	-
11	-	4	0	-
12	**L1**	4	0	-
13	**L3**	4	0	-
14	**1**	2	>99	100:0
15	**1·MeCN**[c]	2	98	100:0
16	**3**	2	>99	100:0
17	**6**	2	50	35:65
18	**8**	2	56	n.d.[d]
19	**1**	1	98	100:0
20	**1·MeCN**[c]	1	50	35:65
21	**3**	1	95	100:0
22	**6**	1	11	10:90
23	**8**	1	30	35:65
24	**1**[e]	1	50	27:73
25	**3**[e]	1	50	17:83

[a]Reaction was performed with imidazolidine-2-one (0.20 mmol) under the indicated ethylene pressure, gold catalyst (0.01 mmol) and AgSbF₆ (0.01 mmol) as chloride abstractor in 1,4-dioxane (1 mL) at 100 °C for 18 h. [b]Conversion was determined by ¹H NMR spectroscopy with anisole as

the internal standard. In brackets the ratio of mono- (**11**) and dihydroaminated (**10**) products [c]In the absence of AgSbF_6. [d]Not determined (n.d). [e]Catalyst loading at 2 mol%.
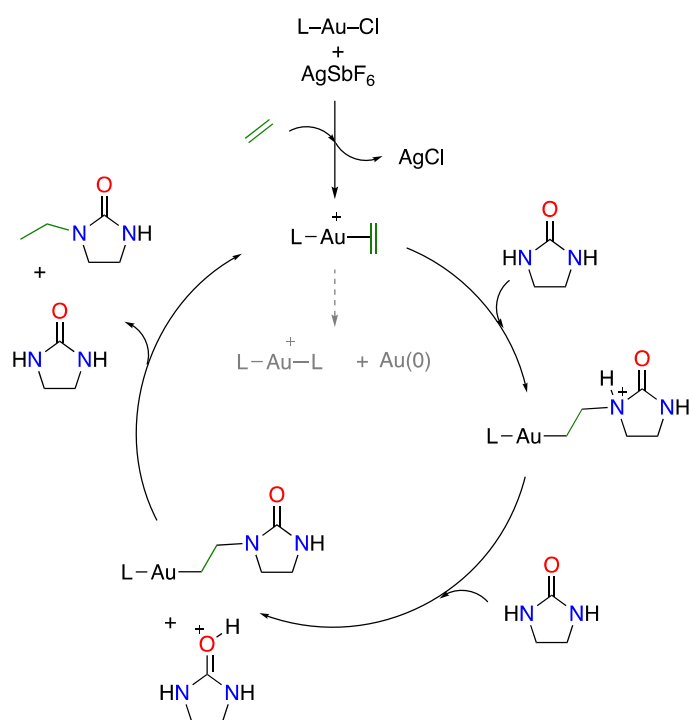
Complexes **1** and **3** reach also full conversion after 18 h when 2 and 1 bar of ethylene pressure was used (Table 2, entries 14, 16, 19 and 21). However, conversion drops to 50% when the catalyst loading is lowered to 2 mol%. Complex **1·MeCN** reaches full conversion with 2 bar of ethylene (Table 2, entry 15) but only 50% conversion under 1 bar of ethylene pressure (Table 2, entry 20). In this case, the presence of acetonitrile may compete with ethylene coordination at low pressure, as we have proved before,[19] decreasing its catalytic activity. Complexes **6** and **8** only reach moderate conversions of ~50% at 2 bar of ethylene pressure (Table 2, entries 17 and 18) and 30% and 11% (Table 2, entries 22 and 23) at 1 bar of ethylene pressure, respectively. For the latter two complexes a mixture of the mono- (**11**) and dihydroaminated (**10**) products was detected by ^{1}H NMR spectroscopy, suggesting that the double hydroamination process proceeds in a stepwise manner.

Complexes **1** and **3** are also able to successfully convert 1-methyl-imdazolidin-2-one into 1-methyl-2-ethylimidazolidin-2-one at 1 bar of ethylene pressure after 18 h at 100 °C, while only traces (<10 %) of the hydroaminated product was observed when 2-oxazolidinone was used as substrate even at 4 bar of ethylene pressure. In contrast, acyclic amide substrates could not be converted. Bulky amines, such as diisopropylamine or *tert*-butylamine, were also tested as substrates using gold(I) complexes **1** and **3**, but no conversion was observed. In these cases, new signals were detected in the $^{31}P\{^{1}H\}$ NMR spectra of the final mixtures that differ from the corresponding gold(I) chloride and gold(I) π-ethylene complexes. For instance, from the reaction of complex **1** with diisopropylamine under catalytic conditions, a single crystal suitable for X-ray diffraction analysis was isolated and analyzed, confirming the coordination of the amine to the electrophilic Au(I) center (Figure S62) to form the corresponding [P–Au–NH^{i}Pr_2]$^{+}$ complex **12**. Surprisingly, even more hindered amines like *N*-benzhydrylpropan-2-amine and tetramethylpiperidine are capable of displacing the ethylene molecule in gold(I) complex **1·C_2H_4** to yield gold-adducts analogous to **12**, as inferred from their corresponding $^{31}P\{^{1}H\}$ and ^{1}H NMR spectra (Figure S55, see Supporting Information for more details). Thus, the extreme steric profile of **L1** does not seem to prevent amine coordination and as such the targeted nucleophilic attack of the amine towards the electrophilic carbon of the coordinated ethylene does not occur, preventing the initiation of the catalytic hydroamination process.

Mechanistic considerations of the gold(I)-catalyzed hydroamination of ethylene.

The gold(I)-catalyzed hydroamination of unsaturated alkenes has been recently studied computationally by Lledós and coworkers.[11g] The proposed mechanism (Scheme 2) was described as a typical π-catalysis activation pathway, involving the coordination of the alkene to the gold(I)
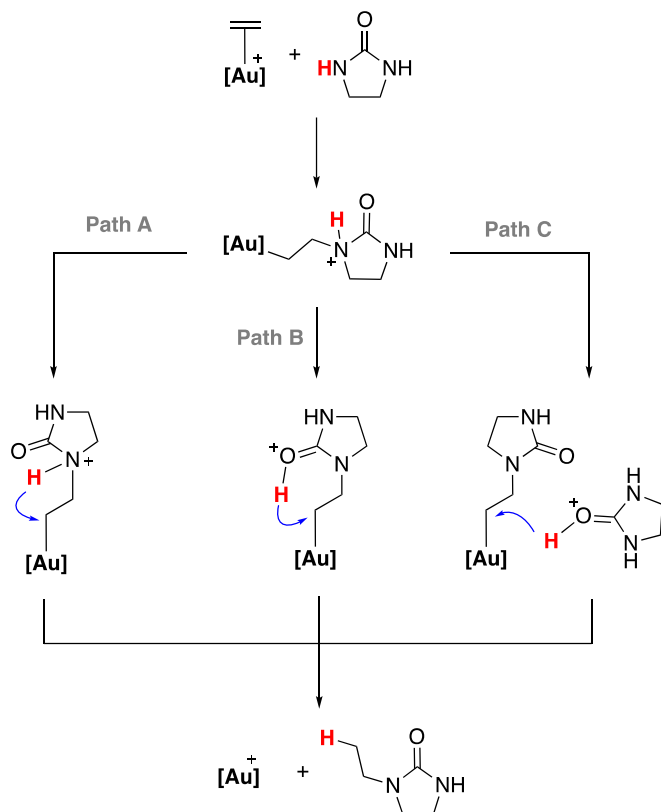
center, followed by the nucleophilic addition of the amide to the activated olefin. The second and final step corresponds to a protodeauration reaction of the corresponding alkenyl gold(I) intermediate assisted by a second amide molecule to generate the hydroaminated product. In this report, we have demonstrated that the use of sterically hindered phosphines is crucial to achieve good activities, which we attribute to the higher stability that they impart to the key π-ethylene intermediates, preventing (or slowing down) the formation of the corresponding [P–Au–P]⁺ complexes as the main deactivation route. In particular, the use of complex **1·C₂H₄**, bearing an extremely bulky phosphine ligand, has given (along with **3·C₂H₄**) the best catalytic activities in this transformation. Therefore, we sought to gain mechanistic insight into this system, by means of kinetic experiments and DFT calculations,[31] to assess whether the previously proposed reaction mechanism[11g] was affected by the steric hindrance of phosphine **L1** in the catalytic process.

Scheme 2. Previously proposed mechanism for the assisted hydroamination of ethylene. Deactivation of the gold(I) precatalyst by formation of [P–Au–P]⁺ and Au(0) nanoparticles is indicated with a dashed grey arrow.

As previously commented, chloride abstraction from the gold(I) chloride precatalyst generates the gold(I)–ethylene complex as the catalytically active species. Then, the nucleophilic addition of imidazolidine-2-one (**9** = Nu) to the electrophilic carbon–carbon double bond constitutes the first step of the process, and presents a barrier of 18.7 kcal/mol (**TS1**) relative to the independently computed reactants (Figure 3). This reaction is an endergonic process, yielding **Int1** at 14.6 kcal/mol. From this step we envisioned three possible mechanistic pathways, two in which the

protodeauration step proceeds directly from the activated N-nucleophile **9** (intramolecular) and one assisted by a second molecule of imidazolidine-2-one (intermolecular) acting as a proton shuttle, as previously reported by Lledós and co-workers. These alternative intramolecular (paths A and B) and intermolecular (path C) routes are summarized in Scheme 3.

Scheme 3. Schematic representation of the three possible mechanistic pathways (paths A–C) for the protodeauration step.

We have computationally explored the three alternative routes depicted in Scheme 3. For the first intramolecular protodeauration process (path A, Figure S64) a direct proton transfer from the nitrogen to the coordinated carbon atom is proposed. An initial rearrangement through a rotation of the coordinated nucleophile (**TS2a**, 19.7 kcal/mol) followed by the proton transfer from the nitrogen to the coordinated carbon atom. The transition state for the proton transfer step (**TS3a**), which leads to the hydroaminated product **11,** was located at 45.9 kcal/mol (Figure S64). This barrier is too high to fit with our experimental observations. Alternatively, an intramolecular proton transfer from the nitrogen to the oxygen atom can be proposed, but the corresponding transition state (**TS2b**) is prohibitively high at 63.0 kcal/mol with respect to the separated reactants. Although the following proton transfer from the oxygen to the coordinated carbon atom (**TS3b**) drops to 23.8 kcal/mol (Figure S65), the overall kinetic penalty highly differs from our experimental results.

On the other hand, for the intermolecular process the proton transfer from the nitrogen atom to the oxygen atom of the second molecule of the imidazolidine-2-one occurs in barrierless fashion, leading to **Int2c** at 18.6 kcal/mol with respect to the separated reactants.[32] Then, a second proton transfer from the protonated nucleophile (**Nu–H**) can occur directly to the coordinated carbon atom (**TS2c**, at 28.3 kcal/mol, Path C in Scheme 3) leading to the final product **11** (Figure S66). This energy barrier (28.3 kcal/mol) is significantly higher than the one found for the intramolecular proton transfer from the oxygen to the coordinated carbon (**TS3b**) in path B. For this reason, we also computed an alternative pathway in which the proton transfer from the nitrogen to the oxygen is assisted by a second molecule of imidazolidine-2-one (path B'). In contrast to the intramolecular scenario in path B (**TS2b**, 63.0 kcal/mol), the intermolecular proton transfer to a second molecule of **9** presents a negligible energy barrier (**TS2b'**, Figure 3). Then, the intramolecular proton transfer to the coordinated carbon atom (**TS3b** = **TS3b'**, at 23.8 kcal/mol) leads to the final hydroaminated product **11** (Figure 3, Path B'). Overall, these data indicate that the two intramolecular processes present unfeasibly high energy barriers of 41.1 and 63.0 kcal/mol, and that a second imidazolidine-2-one molecule acting as a proton shuttle effectively assists the protodeauration step. Path B', in which the protonated imidazolidine-2-one transfers the proton to the oxygen of the coordinated imidazolidine-2-one rather than directly to the carbon atom, presents a substantially lower energy barrier indicating a feasible route. Interestingly, despite its extreme bulkiness, the flexibility of ligand **L1** permits the accommodation of a second molecule of the amide in the cavity generated around the gold center, thus favoring the catalytic process.
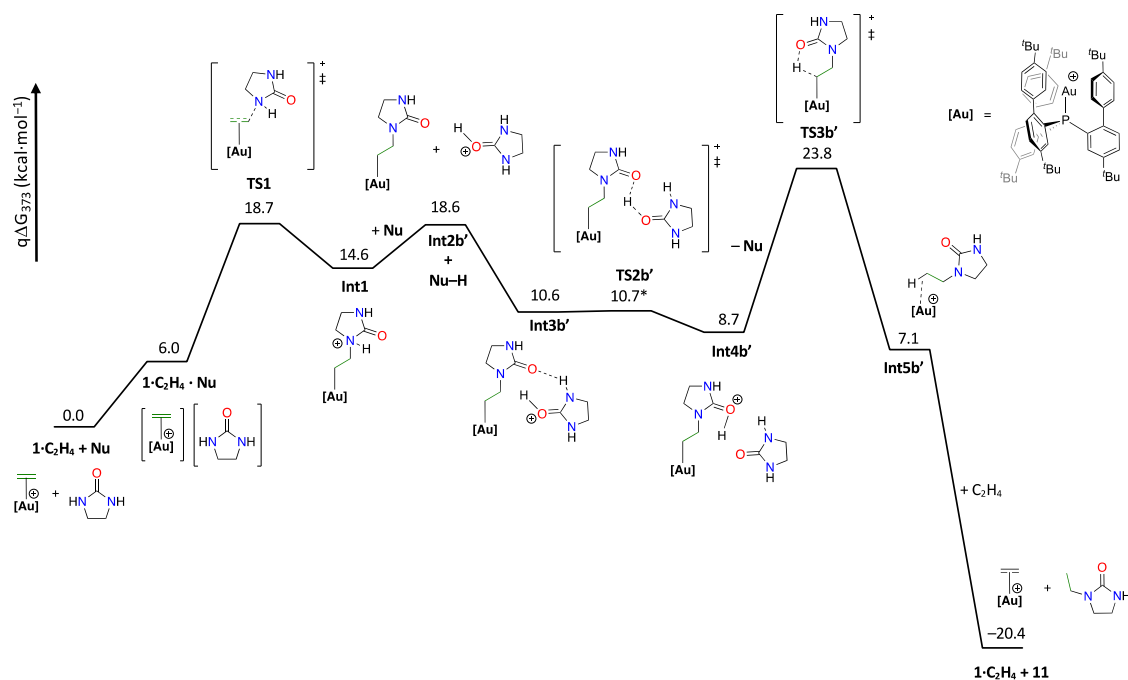

Figure 3. Free energy profile for the Au(I)-catalyzed hydroamination of ethylene with imidazolidine-2-one (**9** = Nu) assisted by a second molecule of imidazolidine-2-one acting as a

proton shuttle (pathway **B'**). (*) Due to an extremely flat surface, the energy difference relative to the preceding minimum was calculated according to electronic energies rather than free energies.

To further support the intermolecular assisted mechanism by experimental means, we monitored by ^{1}H NMR spectroscopy the conversion of 1-methyl-imidazolidine-2-one under catalytic conditions of 5 mol% of complex **1·MeCN** at 100 °C in CDCl₃ under 4 bar of ethylene pressure. The collected data strongly support a second-order dependence on the concentration of 1-methyl-imdazolidine-2-one (Figure 4; see supporting information for more details), thus supporting our mechanistic proposal based on DFT calculations. In addition, the ^{1}H NMR spectra of the reaction showed that the only gold species detected during the course of the reaction is the gold ethylene complex **1·C₂H₄**, corroborating the key role of the gold(I)–ethylene adduct in the gold(I)-catalyzed hydroamination of ethylene and the lack of observable reaction intermediates in path **B'**.
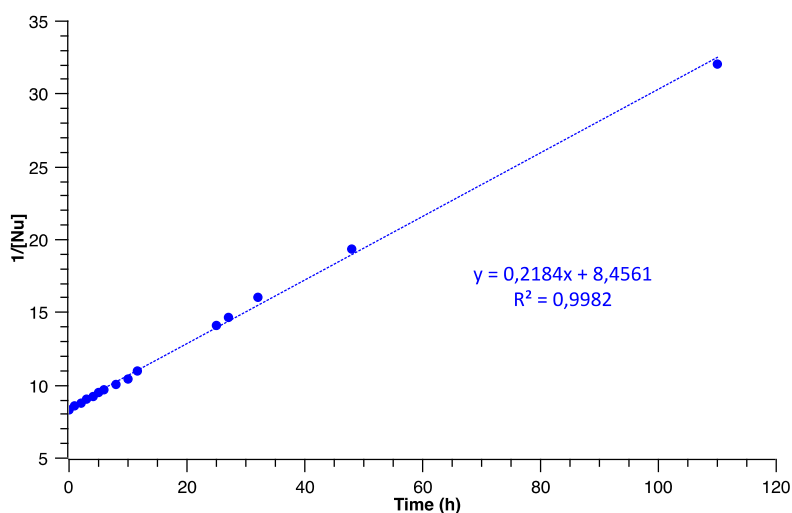

Figure 4. Second-order kinetic representation of the consumption of 1-methyl-imdazolidin-2-one at 100 °C in CDCl₃ under 4 bar of ethylene (k = 6.07 x 10^{-5} s^{-1}).

Conclusions

In summary, we have synthetized and structurally characterized a family of highly unusual dicoordinate gold(I)–ethylene complexes bearing phosphine ligands with variable bulkiness. The use of bulky phosphines is crucial to stabilize the gold(I)–ethylene bond and prevent catalyst decomposition, two key aspects for catalytic performance. In fact, while there is no apparent decomposition for the more sterically hindered complex **1·C₂H₄**, slow decomposition of complexes **2–8·C₂H₄** either in solution or in the solid state is detected. Interestingly, X-ray

diffraction revealed a non-symmetric coordination of ethylene at gold(I) with a slipped η^2-coordination for complex **8·C₂H₄**, further suggesting the lability of this type of coordination. Complexes **1**–**8** have been tested as precatalysts for the underdeveloped Au(I)-catalyzed hydroamination of ethylene. Precatalysts bearing the most sterically demanding phosphines **1** and **3** showed excellent results achieving full conversion within 18 h under only 1 bar of ethylene pressure, highlighting the high catalytic potential of very sterically crowded catalysts. On the other hand, complexes with smaller phosphine ligands afforded little or no conversion in this transformation. In addition, kinetic analysis together with DFT calculations show that the preferred mechanistic pathway involves the assistance of a second molecule of the nucleophile, even when using the more sterically congested cavity-shaped complex **1**.

Experimental part

General considerations. Unless otherwise stated, all reactions and manipulations were carried out under an atmosphere of dry argon or nitrogen using standard Schlenk techniques or in a nitrogen glovebox. Solvents were distilled under inert atmosphere prior to use. Solution ^{1}H, ^{13}C and ^{31}P NMR spectra were recorded on Bruker AMX-300, DRX-400 or DRX-500 spectrometers at 298 K unless otherwise stated. Chemical shifts (δ) are expressed with a positive sign, in parts per million. ^{1}H and ^{13}C chemical shifts reported are referenced internally to residual protio (^{1}H) or deutero (^{13}C) solvent, while ^{31}P chemical shifts are relative to 85% H_3PO_4. The following abbreviations and their combinations are used: br, broad; s, singlet; d, doublet; t, triplet; m, multiplet. The ^{1}H and ^{13}C resonance signals were attributed by means of 2D HSQC and HMBC experiments (Figure 5). For elemental analyses a LECO TruSpec CHN elementary analyzer was utilized. [Au(tht)Cl][33] (tht = tetrahydrothiophene) and all used phosphines (**L1**–**L8**)[18,24] a were prepared according to literature procedures. All other reagents were used as received from commercial suppliers.
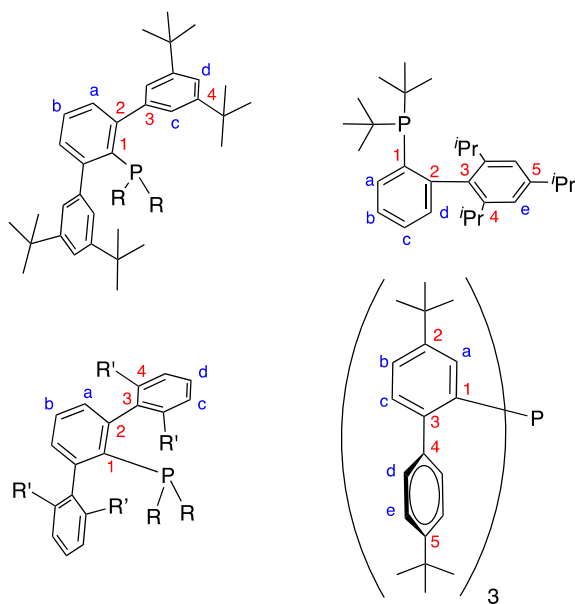
Figure 5. Labeling scheme used for ^{1}H and ^{13}C{^{1}H} NMR assignments.

General synthesis of gold(I) chloride complexes. A solution of the corresponding phosphine (0.470 mmol) in toluene (10 mL) was added over a suspension of [Au(tht)Cl] (150 mg, 0.470 mmol) in toluene (5 mL) at 0 °C. The initial white suspension was stirred for 12 h at rt becoming a clear solution. The solvent was removed under vacuum and the resulting white solid washed with pentane and dried to give the corresponding gold chloride complexes. Complexes **1–6** have been previously reported.[19,21,23b]

Complex 7

Complex **7** was prepared following the general procedure from **L7** (221 mg, 63%). Crystals suitable for X-ray diffraction were grown by slow evaporation of pentane into a dichloromethane solution of complex **7** at –32 °C. **^{1}H NMR** (300 MHz, C$_6$D$_6$, 25 ℃) δ: 7.61 (s, 2H, H$_d$), 7.58 (s, 4H, H$_c$), 7.19–7.02 (m, 3H, H$_a$ + H$_b$), 1.43 (s, 36H, CH$_{3(tBu)}$), 0.50 (d, 6H, $^2J_{HP}$ = 10.0 Hz, PCH$_3$). **^{13}C{^{1}H} NMR** (100 MHz, C$_6$D$_6$, 25 ℃) δ: 152.3 (C$_4$), 148.7 (d, $^2J_{CP}$ = 8 Hz, C$_3$), 141.8 (s, C$_2$), 131.3 (d, $^3J_{PC}$ = 7 Hz, CH$_a$), 130.1 (s, CH$_b$), 129.4 (d, $^1J_{PC}$ = 55 Hz, C$_1$), 124.9 (s, CH$_c$) 122.9 (s, CH$_d$), 35.3 (s, C$_{(tBu)}$), 31.8 (s, CH$_{3(tBu)}$), 17.6 (d, $^1J_{CP}$ = 40 Hz, PCH$_3$). **^{31}P{^{1}H} NMR** (202 MHz, C$_6$D$_6$, 25 ℃) δ: 0.4.

Complex 8

Complex **8** was prepared following the general procedure from **L8** (295 mg, 71%). Crystals suitable for X-ray diffraction were grown by slow evaporation of a concentrated dichloromethane solution of complex **8**. **Anal. Calcd.** for C$_{46}$H$_{67}$AuClP: C, 62.54; H, 7.64. **Found:** C, 62.36; H,

7.27. **^{1}H NMR** (300 MHz, CD_2Cl_2, 25 ℃) δ: 7.56 (d, 2H, $^4J_{HH}$ = 1.7 Hz, CH_d), 7.45 (td, 1H, $^3J_{HH}$ = 7.5 Hz, $^5J_{HP}$ = 1.6 Hz, CH_b), 7.24 (dd, 2H, $^3J_{HH}$ = 7.5 Hz, $^4J_{HP}$ = 3.0 Hz, CH_a), 7.06 (d, 4H, $^4J_{HH}$ = 1.8 Hz, CH_c), 2.12–1.95 (m, 2H, $CH_{(Cy)}$), 1.78–1.55 (m, 10H, $CH_{2(Cy)}$), 1.52–1.45 (m, 2H, $CH_{(Cy)}$), 1.40 (s, 36H, $CH_{3(tBu)}$), 1.35–1.25 (m, 4H, $CH_{2(Cy)}$), 1.19–1.11 (m, 2H, $CH_{2(Cy)}$). 1.10–0.99 (m, 2H, $CH_{2(Cy)}$). **^{13}C{^{1}H} NMR** (100 MHz, CD_2Cl_2, 25 ℃) δ: 151.3 (s, C_4), 150.6 (s, C_2), 142.9 (d, $^3J_{PC}$ = 5 Hz, C_3), 133.4 (d, $^3J_{PC}$ = 7 Hz, CH_a), 129.8 (s, CH_b), 124.5 (s, CH_c), 124.3 (d, $^1J_{PC}$ = 48 Hz, C_1), 123.2 (CH_c), 37.8 (d, $^1J_{PC}$ = 31 Hz, $CH_{(Cy)}$), 35.7 (s, $C_{(tBu)}$), 34.6 (d, $^3J_{PC}$ = 6 Hz, $CH_{2(Cy)}$), 32.1 (s, $CH_{3(tBu)}$), 31.7 (s, $CH_{2(Cy)}$), 27.1 (d, $^2J_{PC}$ = 13 Hz, $CH_{2(Cy)}$), 26.8 (d, $^2J_{PC}$ = 15 Hz, $CH_{2(Cy)}$), 26.3 (s, $CH_{2(Cy)}$). **^{31}P{^{1}H} NMR** (162 MHz, CD_2Cl_2, 25 ℃) δ: 48.8.

General synthesis of gold(I)-ethylene complexes. In a glovebox, a Schlenk flask was charged with silver hexafluoroantimonate (8 mg, 0.022 mmol) in dichloromethane (1 mL). The corresponding gold(I) chloride complex (0.02 mmol) was transferred into a small glass vial and dissolved in dichloromethane (1 mL). The vial solution was loaded into a plastic syringe equipped with a stainless steel needle. Outside the glovebox, the Schlenk flask was cooled down to –30 °C. At this temperature the solution of the gold(I) chloride complex was added to the $AgSbF_6$ suspension while bubbling ethylene. The mixture was allowed to slowly warm up to room temperature, filtered through a short pad of Celite to remove the silver salts, and the solvent was removed under vacuum affording the corresponding gold(I)-ethylene complexes as white solids. Complex **1·C$_2$H$_4$** has been previously reported.[19]

Compound 2·C$_2$H$_4$

Complex **2·C$_2$H$_4$** was prepared following the general procedure from gold(I) chloride complex **2** (13 mg, 78%). **Anal. Calcd.** for $C_{29}H_{37}AuF_6PSb$: C, 41.01; H, 4.39. **Found:** C, 41.08; H, 4.54.
^{1}H NMR (400 MHz, CD_2Cl_2, 25 ℃) δ:7.01 (bs, 6H, m-CH), 5.46 (bs, 4H, $CH_{2(C2H4)}$), 2.66 (bs, 9H, o-CH_3), 2.36 (s, 9H, p-CH_3), 1.86 (bs, 9H, o-CH_3). **^{13}C{^{1}H} NMR** (100 MHz, CD_2Cl_2, 25 ℃) δ: 143.6 (s, p-C), 143.0 (bs, o-C), 132.9 (bs, m-CH), 123.3 (d, $^1J_{CP}$ = 56 Hz, C), 111.2 (d, $^2J_{CP}$ = 9 Hz, $C_{(C2H4)}$), 24.4 (bs, o-CH_3), 21.3 (s, p-CH_3). **^{31}P{^{1}H} NMR** (162 MHz, CD_2Cl_2, 25 ℃) δ: 1.5.
^{1}H NMR (400 MHz, CD_2Cl_2, –30 ℃) δ:7.06 (s, 3H, m-CH), 6.90 (s, 3H, m-CH), 5.43 (bs, 4H, $CH_{2(C2H4)}$), 2.64 (s, 9H, o-CH_3), 2.31 (s, 9H, p-CH_3), 1.78 (s, 9H, o-CH_3). **^{13}C{^{1}H} NMR** (100 MHz, CD_2Cl_2, –30 ℃) δ:143.3 (d, $^3J_{CP}$ = 5 Hz, o-C), 143.0 (s, p-C), 142.2 (d, $^3J_{CP}$ = 16 Hz, o-C), 133.0 (d, $^3J_{CP}$ = 9 Hz, m-CH), 132.0 (d, $^4J_{CP}$ = 10 Hz, m-CH), 122.6 (bs, $CH_{2(C2H4)}$), 122.5 (d, $^1J_{CP}$ = 56 Hz, C), 24.9 (d, $^3J_{CP}$ = 17 Hz, o-CH_3), 24.0 (d, $^3J_{CP}$ = 5 Hz, o-CH_3), 21.0 (s, p-CH_3). **^{1}H NMR** (400 MHz, CD_2Cl_2, –70 ℃) δ: 7.03 (d, 6H, $^4J_{HP}$ = 5.0 Hz, m-CH), 6.87 (s, 6H, m-CH), 5.67 (d, 4H, $^3J_{HP}$ = 2.9 Hz, $CH_{2(C2H4)}$), 2.60 (s, 9H, o-CH_3), 2.28 (s, 9H, p-CH_3), 1.72 (s, 9H, o-CH_3).

Compound 3·C₂H₄

Complex **3·C₂H₄** was prepared following the general procedure from gold(I) chloride complex **3** (16 mg, 89%). Crystals suitable for X-ray diffraction were grown by slow evaporation of pentane into a dichloromethane solution of complex **3·C₂H₄**. **Anal. Calcd.** for $C_{31}H_{49}AuF_6PSb$: C, 42.05; H, 5.58. **Found:** C, 41.83; H, 5.89. **¹H NMR** (400 MHz, CD_2Cl_2, 25 °C) δ: 7.90 (m, 1H, CH_d), 7.64 (m, 2H, $CH_b + CH_c$), 7.29 (s, 2H, CH_e), 7.23 (m, 1H, CH), 4.95 (d, 4H, $^3J_{HP}$ = 2.6 Hz, $CH_{2(C2H4)}$), 3.04 (hept, 1H, $^3J_{HH}$ = 6.9 Hz, $CH_{(iPr)}$), 2.35 (hept, 2H, $^3J_{HH}$ = 6.9 Hz, $CH_{(iPr)}$), 1.45 (d, 18H, $^3J_{HP}$ = 16.5 Hz, $CH_{3(tBu)}$), 1.35 (d, 6H, $^3J_{HH}$ = 6.9 Hz, $CH_{3(iPr)}$), 1.24 (d, 6H, $^3J_{HH}$ = 6.9 Hz, $CH_{3(iPr)}$), 0.94 (d, 6H, $^3J_{HH}$ = 6.9 Hz, $CH_{3(iPr)}$). **¹³C{¹H} NMR** (100 MHz, CD_2Cl_2, 25 °C) δ: 151.9 (s, C_5), 149.0 (s, C_4), 146.8 (d, $^2J_{CP}$ = 15 Hz, C_2), 136.9 (d, $^3J_{CP}$ = 7 Hz, C_3), 135.8 (d, $^3J_{CP}$ = 3 Hz, CH_d), 135.4 (d, $^2J_{CP}$ = 8 Hz, CH_a), 132.5 (d, $^4J_{CP}$ = 2 Hz, CH_c), 128.7 (d, $^3J_{CP}$ = 7 Hz, CH_b), 128.4 (d, $^1J_{CP}$ = 45 Hz, C_1), 123.5 (s, CH_e), 110.9 (d, $^2J_{CP}$ = 8 Hz, $C_{(C2H4)}$), 39.9 (d, $^1J_{CP}$ = 24 Hz, $C_{(tBu)}$), 34.7 (s, p-$CH_{(iPr)}$), 31.6 (s, o-$CH_{(iPr)}$), 31.6 (s, $CH_{3(tBu)}$) 26.0 (s, $CH_{3(iPr)}$), 24.6 (s, $CH_{3(iPr)}$), 23.8 (s, $CH_{3(iPr)}$). **³¹P{¹H} NMR** (162 MHz, CD_2Cl_2, 25 °C) δ: 65.6.

Compound 4·C₂H₄

Complex **4·C₂H₄** was prepared following the general procedure from gold(I) chloride complex **4** (13 mg, 71%). **Anal. Calcd.** for $C_{34}H_{47}AuF_6PSb$: C, 44.42; H, 5.15. **Found:** C, 44.48; H, 5.31. **¹H NMR** (400 MHz, CD_2Cl_2, 25 °C) δ: 7.64 (td, 1H, $^3J_{HH}$ = 7.6 Hz, $^5J_{HP}$ = 1.9 Hz, CH_b), 7.55 (t, 2H, $^3J_{HH}$ = 7.3 Hz, CH_d), 7.40 (d, 4H, $^3J_{HH}$ = 7.3 Hz, CH_c), 7.26 (dd, 2H, $^3J_{HH}$ = 7.6 Hz, $^4J_{HP}$ = 3.7 Hz, CH_a), 4.85 (d, 4H, $^3J_{HP}$ = 3.0 Hz, $CH_{2(C2H4)}$), 2.45 (hept, $^3J_{HH}$ = 6.8 Hz, 4H, $CH_{(iPr)}$), 1.46 (d, $^3J_{HP}$ = 10.7 Hz, 6H, PCH_3), 1.31 (d, 2H, $^3J_{HH}$ = 6.8 Hz, 12H, $CH_{3(iPr)}$), 1.06 (d, 2H, $^3J_{HH}$ = 6.8 Hz, 12H, $CH_{3(iPr)}$). **¹³C{¹H} NMR** (100 MHz, CD_2Cl_2, 25 °C) δ: 147.8 (s, C_4), 146.2 (d, $^2J_{PC}$ = 12 Hz, C_2), 138.2 (d, $^3J_{PC}$ = 6 Hz, C_3), 133.7 (d, $^3J_{PC}$ = 8 Hz, CH_a), 132.0 (s, CH_b), 130.4 (s, CH_d), 127.9 (d, $^1J_{CP}$ = 60 Hz C_1), 124.6 (s, CH_c), 110.3 (d, $^2J_{CP}$ = 9 Hz, $CH_{2(C2H4)}$), 32.0 (s, $CH_{(iPr)}$), 25.6 (s, $CH_{3(iPr)}$), 23.2 (s, $CH_{3(iPr)}$), 16.2 (d, $^2J_{CP}$ = 37 Hz, PCH_3). **³¹P{¹H} NMR** (162 MHz, CD_2Cl_2, 25 °C) δ: 4.3.

Compound 5·C₂H₄

Complex **5·C₂H₄** was prepared following the general procedure from gold(I) chloride complex **5** (9 mg, 53%). **¹H NMR** (400 MHz, CD_2Cl_2, 25 °C) δ: 7.72 (td, 1H, $^3J_{HH}$ = 7.6 Hz, $^5J_{HP}$ = 1.9 Hz, CH_b), 7.36 (t, 2H, $^3J_{HH}$ = 7.3 Hz, CH_d), 7.28 (d, 4H, $^3J_{HH}$ = 7.3 Hz, CH_c), 7.15 (dd, 2H, $^3J_{HH}$ = 7.6 Hz, $^4J_{HP}$ = 3.6 Hz, CH_a), 5.00 (bs, 4H, $CH_{2(C2H4)}$), 2.04 (s, 12H, $CH_{3(Xyl)}$), 1.49 (d, 2H, $^2J_{HP}$ = 10.4 Hz, PCH_3). **¹³C{¹H} NMR** (100 MHz, CD_2Cl_2, 25 °C) δ: 147.8 (d, $^2J_{PC}$ = 13 Hz, C_2), 140.7 (s, C_3), 137.3 (s, C_4), 134.3 (s, CH_b), 132.4 (d, $^3J_{PC}$ = 8 Hz, CH_a), 129.3 (s, CH_d), 129.0 (s, CH_c), 125.6 (s, C_1), 111.5 (s, $CH_{2(C2H4)}$), 21.8 (s, $CH_{3(Xyl)}$), 16.0 (d, $^2J_{CP}$ = 37 Hz, PCH_3). **³¹P{¹H} NMR**

(162 MHz, CD$_2$Cl$_2$, 25 ºC) δ: 4.1. **^{1}H NMR** (400 MHz, CD$_2$Cl$_2$, –30 ºC) δ: 7.72 (td, 1H, $^3J_{HH}$ = 7.6 Hz, $^5J_{HP}$ = 1.9 Hz, CH$_b$), 7.37 (t, 2H, $^3J_{HH}$ = 7.5 Hz, CH$_d$), 7.28 (d, 4H, $^3J_{HH}$ = 7.5 Hz, CH$_c$), 7.14 (dd, 2H, $^3J_{HH}$ = 7.6 Hz, $^4J_{HP}$ = 3.7 Hz, CH$_a$), 5.36 (bs, 4H, CH$_{2(C2H4)}$), 2.02 (s, 12H, CH$_{3(Xyl)}$), 1.48 (d, 2H, $^2J_{HP}$ = 10.7 Hz, PCH$_3$). **^{13}C{^{1}H} NMR** (100 MHz, CD$_2$Cl$_2$, –30 ºC) δ: 147.1 (d, $^2J_{PC}$ = 12 Hz, C$_2$), 140.1 (d, $^3J_{PC}$ = 7 Hz, C$_3$), 136.9 (s, C$_4$), 134.0 (s, CH$_b$), 131.8 (d, $^3J_{PC}$ = 7 Hz, CH$_a$), 128.9 (s, CH$_d$), 128.5 (s, CH$_c$), 125.1 (d, $^1J_{PC}$ = 62 Hz. C$_1$), 120.9 (bs, CH$_{2(C2H4)}$), 21.6 (s, CH$_{3(Xyl)}$), 15.6 (d, $^2J_{CP}$ = 37 Hz, PCH$_3$).

Compound 6·C$_2$H$_4$

Complex **6·C$_2$H$_4$** was prepared following the general procedure from gold(I) chloride complex **6** (16 mg, 87%). **Anal. Calcd.** for C$_{34}$H$_{43}$AuF$_6$PSb: C, 44.61; H, 4.73. **Found:** C, 44.68; H, 4.99. **^{1}H NMR** (400 MHz, CD$_2$Cl$_2$, 25 ºC) δ: 7.69 (td, 1H, $^3J_{HH}$ = 7.6 Hz, $^5J_{HP}$ = 1.8 Hz, CH$_b$), 7.40–7.22 (m, 6H, CH$_d$ + CH$_c$), 7.21–7.13 (m, 2H, CH$_a$), 4.86 (d, 4H, $^3J_{HP}$ = 2.8 Hz, CH$_{2(C2H4)}$), 2.45–2.28 (m, 2H, CH$_{(Cy)}$), 2.08 (s, 12H, CH$_{3(Xyl)}$), 1.93–1.85 (m, 2H, CH$_{2(Cyp)}$), 1.76–1.57 (m, 6H, CH$_{2(Cyp)}$), 1.56–1.43 (m, 4H, CH$_{2(Cyp)}$), 1.40–1.19 (m, 4H, CH$_{2(Cyp)}$). **^{13}C{^{1}H} NMR** (100 MHz, CD$_2$Cl$_2$, 25 ºC) δ: 148.2 (d, $^2J_{PC}$ = 10 Hz, C$_2$), 140.9 (bs, C$_3$), 137.8 (s, C$_4$), 133.4 (s, CH$_a$), 133.2 (s, CH$_b$), 129.2 (s, CH$_c$), 128.7 (s, CH$_d$), 128.7 (d, $^1J_{PC}$ = 50 Hz, C$_1$), 111.0 (d, $^2J_{CP}$ = 9 Hz, CH$_{2(C2H4)}$), 38.3 (d, $^1J_{PC}$ = 31 Hz, CH$_{(Cyp)}$), 36.3 (d, $^3J_{PC}$ = 8 Hz, CH$_{2(Cyp)}$), 32.8 (d, $^3J_{PC}$ = 6 Hz, CH$_{2(Cyp)}$), 25.8 (d, $^2J_{PC}$ = 12 Hz, CH$_{2(Cyp)}$), 25.6 (d, $^2J_{PC}$ = 14 Hz, CH$_{2(Cyp)}$), 21.9 (s, CH$_{3(Xyl)}$). **^{31}P{^{1}H} NMR** (162 MHz, CD$_2$Cl$_2$, 25 ºC) δ: 57.6. **^{1}H NMR** (400 MHz, CD$_2$Cl$_2$, –30 ºC) δ: 7.71 (td, 1H, $^3J_{HH}$ = 7.6 Hz, $^5J_{HP}$ = 1.9 Hz, CH$_b$), 7.49–7.38 (m, 2H, CH$_d$), 7.34–7.23 (m, 2H, CH$_c$), 7.23–7.17 (m, 2H, CH$_c$), 7.11–7.04 (m, 2H, CH$_a$), 4.86 (d, 4H, $^3J_{HP}$ = 2.8 Hz, CH$_{2(C2H4)}$), 2.43–2.25 (m, 2H, CH$_{(Cy)}$), 2.08 (s, 12H, CH$_{3(Xyl)}$), 1.94–1.84 (m, 2H, CH$_{2(Cyp)}$), 1.79–1.45 (m, 10H, CH$_{2(Cyp)}$), 1.40–1.14 (m, 4H, CH$_{2(Cyp)}$). **^{13}C{^{1}H} NMR** (100 MHz, CD$_2$Cl$_2$, –30 ºC) δ: 147.9 (s, C$_2$), 147.3 (d, $^2J_{PC}$ = 19 Hz, C$_2$), 141.8 (s, C$_3$), 139.1 (s, C$_3$), 137.5 (s, C$_4$), 137.3 (s, C$_4$), 133.2 (d, $^4J_{PC}$ = 7 Hz, CH$_a$), 133.1 (s, CH$_b$), 132.0 (d, $^4J_{PC}$ = 7 Hz, CH$_a$), 129.5 (s, CH$_c$), 129.2 (s, CH$_d$), 128.8 (d, $^1J_{PC}$ = 46 Hz, C$_1$), 127.7 (s, CH$_c$), 111.0 (d, $^2J_{CP}$ = 9 Hz, CH$_{2(C2H4)}$), 37.6 (d, $^1J_{PC}$ = 32 Hz, CH$_{(Cyp)}$), 35.9 (d, $^3J_{PC}$ = 8 Hz, CH$_{2(Cyp)}$), 32.3 (d, $^3J_{PC}$ = 6.5 Hz, CH$_{2(Cyp)}$), 25.2 (d, $^2J_{PC}$ = 12 Hz, CH$_{2(Cyp)}$), 25.1 (d, $^2J_{PC}$ = 14 Hz, CH$_{2(Cyp)}$), 21.8 (s, CH$_{3(Xyl)}$), 21.3 (s, CH$_{3(Xyl)}$).

Compound 7·C$_2$H$_4$

Complex **7·C$_2$H$_4$** was prepared following the general procedure from gold(I) chloride complex **7** (12 mg, 63%). **Anal. Calcd.** for C$_{38}$H$_{55}$AuF$_6$PSb: C, 46.79; H, 5.68. **Found:** C, 46.71; H, 5.94. **^{1}H NMR** (400 MHz, CD$_2$Cl$_2$, 25 ºC) δ: 7.77–7.65 (m, 1H, CH$_b$), 7.64 (t, 2H, $^3J_{HH}$ = 1.7 Hz, CH$_d$), 7.43 (dd, 2H, $^3J_{HH}$ = 7.6 Hz, $^4J_{HP}$ = 3.9 Hz, CH$_a$), 7.25 (d, 4H, $^4J_{HH}$ = 1.7 Hz, CH$_c$), 5.16 (s, 4H, CH$_{2(C2H4)}$), 1.60 (d, 2H, $^2J_{HP}$ = 10.7 Hz, PCH$_3$), 1.41 (s, 36H, CH$_{3(tBu)}$).**^{13}C{^{1}H} NMR** (100 MHz,

CD$_2$Cl$_2$, 25 ºC) δ: 152.6 (s, C$_4$), 150.3 (s, $^2J_{CP}$ = 11 Hz, C$_3$), 141.1 (d, $^3J_{CP}$ = 6 Hz, C$_2$), 132.9 (d, $^3J_{CP}$ = 8 Hz, CH$_a$), 132.1 (s, CH$_b$), 125.5 (d, $^1J_{PC}$ = 60 Hz, C$_1$), 125.0 (s, CH$_d$), 123.5 (s, CH$_d$), 111.8 (bs, CH$_{2(C2H4)}$), 35.6 (s, C$_{(tBu)}$), 31.9 (s, CH$_{3(tBu)}$), 18.4 (d, $^2J_{CP}$ = 37 Hz, PCH$_3$). **^{31}P{^{1}H} NMR** (162 MHz, CD$_2$Cl$_2$, 25 ºC) δ: 9.4. **^{1}H NMR** (400 MHz, CD$_2$Cl$_2$, –30 ºC) δ: 7.71 (td, 1H, $^3J_{HH}$ = 7.7 Hz, $^5J_{HP}$ = 1.7 Hz, CH$_b$), 7.59 (t, 2H, $^3J_{HH}$ = 1.7 Hz, CH$_d$), 7.43 (dd, 2H, $^3J_{HH}$ = 7.7 Hz, $^4J_{HP}$ = 3.8 Hz, CH$_a$), 7.22 (d, 4H, $^4J_{HH}$ = 1.8 Hz, CH$_c$), 5.35 (s, 4H, CH$_{2(C2H4)}$), 1.56 (d, 2H, $^2J_{HP}$ = 10.4, PCH$_3$), 1.37 (s, 36H, CH$_{3(tBu)}$). **^{13}C{^{1}H} NMR** (100 MHz, CD$_2$Cl$_2$, –30 ºC) δ: 151.9 (s, C$_4$), 149.9 (s, $^2J_{CP}$ = 11 Hz, C$_3$), 140.6 (s, $^3J_{CP}$ = 7 Hz, C$_2$), 132.3 (d, $^3J_{CP}$ = 7 Hz, CH$_a$), 131.7 (s, CH$_b$), 125.0 (d, $^1J_{PC}$ = 62 Hz, C$_1$), 124.6 (s, CH$_d$), 123.0 (s, CH$_d$), 120.5 (s, CH$_{2(C2H4)}$), 35.2 (s, C$_{(tBu)}$), 31.4 (s, CH$_{3(tBu)}$), 18.0 (d, $^2J_{CP}$ = 37 Hz, PCH$_3$).

Compound 8·C$_2$H$_4$

Complex **8·C$_2$H$_4$** was prepared following the general procedure from gold(I) chloride complex **8** (21 mg, 93%). Crystals suitable for X-ray diffraction were grown by slow diffusion of pentane into a dichloromethane solution of complex **8·C$_2$H$_4$**. **Anal. Calcd.** for C$_{48}$H$_{71}$AuF$_6$PSb: C, 51.86; H, 6.44. **Found:** C, 51.92; H, 6.64. **^{1}H NMR** (400 MHz, CD$_2$Cl$_2$, 25 ºC) δ: 7.65 (s, 2H, CH$_d$), 7.55 (td, 1H, $^3J_{HH}$ = 7.7 Hz, $^5J_{HP}$ = 1.8 Hz, CH$_b$), 7.26 (bs, 2H, CH$_a$), 7.13 (d, 4H, $^4J_{HH}$ = 1.8 Hz, CH$_c$), 4.77 (s, 4H, CH$_{2(C2H4)}$), 2.37–2.21 (m, 2H, CH$_{(Cy)}$), 1.89–1.65 (m, 10H, CH$_{2(Cy)}$), 1.42 (s, 36H, CH$_{3(tBu)}$), 1.22–1.04 (m, 10H, CH$_{2(Cy)}$). **^{13}C{^{1}H} NMR** (100 MHz, CD$_2$Cl$_2$, 25 ºC) δ: 152.8 (bs, C$_4$), 149.9 (s, C$_3$), 149.8 (s, C$_2$), 133.9 (s, CH$_a$), 131.4 (s, CH$_b$), 123.9 (bs, CH$_c$ + CH$_d$), 122.8 (d, $^1J_{PC}$ = 50 Hz, C$_1$), 109.0 (s, CH$_{2(C2H4)}$), 38.6 (d, $^1J_{PC}$ = 28 Hz, CH$_{(Cy)}$), 35.7 (s, C$_{(tBu)}$), 34.3 (d, $^3J_{PC}$ = 6 Hz, CH$_{2(Cy)}$), 31.9 (s, CH$_{3(tBu)}$), 31.9 (s, CH$_{2(Cy)}$), 26.9 (d, $^2J_{PC}$ = 16 Hz, CH$_{2(Cy)}$), 26.7 (d, $^2J_{PC}$ = 13 Hz, CH$_{2(Cy)}$), 26.0 (s, CH$_{2(Cy)}$). **^{31}P{^{1}H} NMR** (162 MHz, CD$_2$Cl$_2$, 25 ºC) δ: 55.4. **^{1}H NMR** (400 MHz, CD$_2$Cl$_2$, –30 ºC) δ: 7.60 (s, 2H, CH$_d$), 7.54 (td, 1H, $^3J_{HH}$ = 7.6 Hz, $^5J_{HP}$ = 1.8 Hz, CH$_b$), 7.31 (d, 1H, $^3J_{HH}$ = 7.6 Hz, CH$_a$), 7.19 (dd, 1H, $^3J_{HH}$ = 7.6 Hz, $^4J_{HP}$ = 4.3 Hz, CH$_a$), 7.10 (s, 2H, CH$_c$), 7.08 (s, 2H, CH$_c$), 4.69 (d, 4H, $^3J_{HP}$ = 2.6 Hz, CH$_{2(C2H4)}$), 2.26–2.07 (m, 2H, CH$_{(Cy)}$), 1.84–1.58 (m, 10H, CH$_{2(Cy)}$), 1.38 (s, 18H, CH$_{3(tBu)}$), 1.37 (s, 18H, CH$_{3(tBu)}$), 1.23–0.98 (m, 10H, CH$_{2(Cy)}$). **^{13}C{^{1}H} NMR** (100 MHz, CD$_2$Cl$_2$, –30 ºC) δ: 152.3 (s, C$_4$), 151.0 (s, C$_4$), 149.1 (s, C$_3$), 149.0 (s, C$_2$), 142.7 (s, C$_3$), 140.4 (s, C$_2$), 133.6 (d, $^3J_{PC}$ = 6 Hz, CH$_a$), 133.2 (d, $^3J_{PC}$ = 6 Hz, CH$_a$), 131.0 (s, CH$_b$), 124.3 (s, CH$_{cc}$), 123.9 (s, CH$_d$), 122.8 (s, CH$_c$), 122.6 (d, $^1J_{PC}$ = 50 Hz, C$_1$), 109.0 (d, $^2J_{PC}$ = 8 Hz, CH$_{2(C2H4)}$), 37.2 (d, $^1J_{PC}$ = 29 Hz, CH$_{(Cy)}$), 35.5 (s, C$_{(tBu)}$), 35.2 (s, C$_{(tBu)}$), 33.9 (d, $^3J_{PC}$ = 5 Hz, CH$_{2(Cy)}$), 31.5 (s, CH$_{3(tBu)}$), 31.3 (s, CH$_{2(Cy)}$), 26.3 (d, $^2J_{PC}$ = 15 Hz, CH$_{2(Cy)}$), 26.2 (d, $^2J_{PC}$ = 15 Hz, CH$_{2(Cy)}$), 25.5 (s, CH$_{2(Cy)}$).

Synthesis of gold(I)-amine complex 12. A solution of complex **1** (32 mg, 0.02 mmol) in dichloromethane (1 mL) in the presence of diisopropylamine (5 mL, 0.03 mmol) was added to a

suspension of silver hexafluoroantimonate (12 mg, 0.03 mmol) in dichloromethane (1 mL) at rt. The mixture was stirred for 30 min, filtered through a short pad of Celite to remove the silver salts, and the solvent was removed under vacuum affording complex **12** as white solid (24 mg, 87%). Crystals suitable for X-ray diffraction were grown by slow evaporation of diffusion into a dichloromethane solution of complex **12**. **^{1}H NMR** (500 MHz, CD$_2$Cl$_2$, 25 ℃) δ: 7.73 (d, 3H, $^3J_{HH}$ = 8.1 Hz, H$_b$), 7.51–7.35 (m, 6H, H$_a$, H$_c$), 7.23 (d, 6H, $^3J_{HH}$ = 8.0 Hz, H$_e$), 6.88 (d, 6H, $^3J_{HH}$ = 8.0 Hz, H$_d$), 2,73 (hept, 1H, $^3J_{HH}$ = 6.3 Hz, CH$_{(iPr)}$), 2.16 (bs, 1H, CH$_{(iPr)}$), 1.26 (s, 27H, CH$_{3(tBu3)}$), 1.20 (s, 27H, CH$_{3(tBu3)}$), 0.65 (d, 3H, $^3J_{HH}$ = 6.3 Hz, CH$_{3(iPr)}$), 0.53 (d, 3H, $^3J_{HH}$ = 6.3 Hz, CH$_{3(iPr)}$), 0.51 (d, 3H, $^3J_{HH}$ = 6.3 Hz, CH$_{3(iPr)}$), 0.45 (d, 3H, $^3J_{HH}$ = 6.3 Hz, CH$_{3(iPr)}$). **^{13}C{^{1}H} NMR** (125 MHz, CD$_2$Cl$_2$, 25 ℃) δ: 151.8 (d, $^3J_{CP}$ = 8 Hz, C$_2$), 151.4 (s, C$_5$), 143.6 (d, $^2J_{CP}$ = 15 Hz, C$_3$), 138.7 (d, $^3J_{CP}$ = 6 Hz, C$_4$), 134.9 (d, $^3J_{CP}$ = 10 Hz, CH$_a$ or CH$_c$), 133.9 (d, $^3J_{CP}$ = 8 Hz, CH$_a$ or CH$_c$), 130.2 (s, CH$_d$), 129.6 (d, $^4J_{CP}$ = 3 Hz, CH$_b$), 127.8 (d, $^1J_{CP}$ = 62 Hz, C$_1$), 126.0 (s, CH$_e$), 49.5 (s, CH$_{(iPr)}$), 49.1 (s, CH$_{(iPr)}$), 35.3 (s, C$_{(tBu3)}$), 35.1 (s, C$_{(tBu3)}$), 31.6 (s, CH$_{3(tBu3)}$), 31.3 (s, CH$_{3(tBu3)}$), 25.6 (s, CH$_{3(iPr)}$), 23.8 (s, CH$_{3(iPr)}$). **^{31}P{^{1}H} NMR** (202 MHz, CD$_2$Cl$_2$, 25 ℃) δ: 11.1.

General procedure for the gold(I)-catalyzed hydroamination of ethylene. A mixture of amide (0.20 mmol), gold chloride complex (0.01 mmol) and silver hexafluoroantimoniate (4 mg, 0.01 mmol) in dioxane (1 mL) was placed in a Fischer Porter tube together with a magnetic stirring bar under nitrogen atmosphere. The tube was freeze-pumped to remove the nitrogen gas, filled with the indicated ethylene pressure and stirred at 100 °C for 18 h. After this time, the mixture was cooled down to rt, diluted in CH$_2$Cl$_2$ (5 mL) and anisole (22 mL, 0.20 mmol) was added as internal standard. The mixture was then filtered through a short pad of celite, the solvents removed under reduced pressure and the sample analyzed by NMR spectroscopy in CDCl$_3$.

Supporting Information

　　　NMR spectra, kinetic studies, X-ray structural data, computational details (PDF).

　　　Cartesian coordinates (XYZ)

Accession codes:

1 Hammer, B.; Norskov, J. K. *Nature* **1995**, *376*, 238–240.

2 a) Teles, J. H.; Brode, S.; Chabanas, M. *Angew. Chem. Int. Ed.* **1998**, *37*, 1415–1418; b) Hashmi, A. S. K.; Schwarz, L.; Choi, J.-H.; Frost, T. M. *Angew. Chem. Int. Ed.* **2000**, *39*, 2285–2288; c) Hashmi, A. S. K. *Gold Bull.* **2004**, *37*, 51–65; d) Hashmi, A. S. K.; Toste, F. D. *Modern Gold Catalyzed Synthesis*, Wiley-VCH, **2012**; e) Toste, F. D.; Michelet, V. *Gold Catalysis: An Homogeneous Approach,* Imperial College Press, **2014**; f) Slaughter L. M. *Homogeneous Gold Catalysis*, Springer **2015**; g) Wang, T.; Hashmi, A. S. K. *Chem. Rev.* **2021**, *121*, 8948–8978; h) Campeau, D.; Rayo, D. F. K.; Mansour, A.; Murativ, K.; Gagosz, F. *Chem. Rev.* 2021, **121**, 8756–8867.

3 a) Fürstner A. *Chem. Soc. Rev.* **2009**, *38*, 3208–3221; b) Krause, N.; Winter, C. *Chem. Rev.* **2011**, *111*, 1994–2009; c) Corma, A.; Leyva-Pérez, A.; Sabater, M. J. *Chem. Rev.* **2011**, *111*, 1657–1712; d) Rudolph, M.; Hashmi, A. S. K. *Chem. Soc. Rev.* **2012**, *41*, 2448–2462; e) Chiarucci, M.; Bandini, M. *Beilstein J. Org. Chem.* **2013**, *9*, 2586–2614; f) Braun I.; Asiri, A. M.; Hashmi, A. S. K. *ACS Catal.* **2013**, *3*, 1902–1907; g) Friend, C. M.; Hashmi, A. S. K. *Acc. Chem. Res.* **2014**, *47*, 729–730; h) Soriano, E.; Fernández, I. *Chem. Soc. Rev.* **2014**, *43*, 3041–3105; i) Obradors, C.; Echavarren, A. M. *Chem. Commun.* **2014**, *50*, 16–28; j) Dorel, R.; Echavarren, A. M. *Chem. Rev.* **2015**, *115*, 9028–9072; k) Halliday, C. J. V.; Lynam, M. *Dalton Trans.* **2016**, *45*, 12611–12626; l) Mascareñas, J. L.; Varela, I.; López, F. *Acc. Chem. Res.* **2019**, *52*, 465–479; m) Zucarello, G.; Zanini, M.; Echavarren, A. M. *Isr. J. Chem.* **2020**, *60*, 360–372.

4 a) Müller, T. E.; Hultzsch, K. C.; Yus, M.; Foubelo, F.; Tada, M. *Chem. Rev.* **2008**, *108*, 3795–3892; b) Huang, K.; Arndt, M.; Gooßen, K.; Heydt, H.; Gooßen, L. J. *Chem. Rev.* **2015**, *115*, 2595–2697; c) Patel, M.; Saunthwal, R. K.; Verma, A. K. *Acc. Chem. Res.* **2017**, *50*, 240–254. d) Streiff, S.; Jérome, F. *Chem. Soc. Rev.* **2021**, *50*, 1512–1521.

5 a) Yang, Y.; Shi, S.-L.; Niu, D.; Liu, P.; Buchwald, S. L. *Science* **2015**, *349*, 62–66; b) Pirnot, M. T.; Wang, Y.-M.; Buchawld, S. L. *Angew. Chem. Int. Ed.* **2015**, *55*, 48–57; c) Tafazolian, H.; Schmidt, J. A. R. *Chem. Eur. J.* **2017**, *23*, 1507–1511; d) Yang, X.-H.; Lu, A.; Dong, V. M. *J. Am. Chem. Soc.* **2017**, *139*, 14049–14052; e) Yang S.; Li, Q.-Z.; Xu, C.; Xu, Q.; Shi, M. *Chem. Sci.* **2018**, *9*, 5074–5081; f) Lepori, C.; Bernoud, E.; Guillot, R.; Tobisch, S.; Hannedouche, J. *Chem. Eur. J.* **2019**, *25*, 835–844; g) Tran, G.; Shao, W.; Mazet, C. *J. Am. Chem. Soc.* **2019**, *141*, 14814–14822; h) Xi, Y.; Ma, S.; Hartwig, J. F. *Nature* **2020**, *588*, 254–261; i) Foster, D.; Gao, P.; Zhang, Z.; Sipos, G.; Sobolev, A. N.; Nealon, G.; Falviene, L.; Cavallo, L.; Dorta, R. *Chem. Sci.* **2021**, *12*, 3751–3767.

6 a) Bernoud, E.; Lepori, C.; Mellah, M.; Schulz, E.; Hannedouche, J. *Catal. Sci. Technol.* **2015**, *5*, 2017–2037; b) Peng, X.; Kaga, A.; Hirao, H.; Chiba, S. *Org. Chem. Front.* **2016**, *3*, 609–613; c) Yu, Z.-L.; Cheng, Y.-F.; Jiang, N.-C.; Wang, J.; Fan, L.-W.; Yuan, Y.; Li, Z.-L.; Gu, Q.-S.;

Liu, X.-Y. *Chem. Sci.* **2020**, *11*, 5987–5993; d) Kim, K.; Park, S.; Lee, Y. *Eur. J. Org. Chem.* **2021**, 125–137.

7 a) Widenhoefer, R. A.; Han, X. *Eur. J. Org. Chem.* **2006**, 4555–4563; b) Leung, C. H.; Baron, M.; Biffis, A. *Catalysts* **2020**, *10*, 1210.

8 a) Mizushima, E.; Hayashi, T.; Tanaka, M. *Org. Lett.* **2003**, *5*, 3349–3352; b) Kramer, S.; Dooleweerdt, K.; Lindhardt, A. T.; Rottländer, M.; Skrydstrup, T. *Org. Lett.* **2009**, *11*, 4208–4211; c) Patil, N. T.; Lakshmi, P. G. V. V.; Singh, V. *Eur. J. Org. Chem.* **2010**, 4719–4731; d) Alvarado, E.; Badaj, A. C.; Larocque, T. G.; Lavoie, G. G. *Chem. Eur. J.* **2012**, *18*, 12112–12121; e) Siewert, J.-E.; Schumann, A.; Fischer, M.; Schmidt, C.; Taeufer, T.; Hering-Junghans, C. *Dalton Trans.* **2020**, *49*, 12354–12364; f) Jia, T.; Fan S.; Li, F.; Ye, X.; Zhang, W.; Song, Z.; Shi, X. *Org. Lett.* **2021**, *23*, 6019–6023.

9 For examples of Au(I)-catalyzed intermolecular hydroamination of allenes see: a) Nishina, N.; Yamamoto, Y. *Angew. Chem. Int. Ed.* **2006**, *45*, 3314–3317; b) LaLonde, R. L.; Sherry, B. D.; Kang, E. J.; Toste, F. D. *J. Am. Chem. Soc.* **2007**, *129*, 2452–2453; c) Wang, Z. J.; Benitez, D.; Tkatchouk, E.; Goddard III, W. A.; Toste, F. D. *J. Am. Chem. Soc.* **2010**, *132*, 13064–13071; d) Kinjo, R.; Donnadieu, B.; Bertrand, G. *Angew. Chem. Int. Ed.* **2011**, *50*, 5560–5563; e) Couce-Rios, A.; Kovács, G.; Ujaque, G.; Lledós, A. *ACS Catal.* **2015**, *5*, 815–829

10 For examples of Au(I)-catalyzed hydroamination of dienes see: a) Brouwer, C.; He, C. *Angew. Chem. Int. Ed.* **2006**, *45*, 1744–1747; b) Kovács, G.; Ujaque, G.; Lledós, A. *J. Am. Chem. Soc.* **2008**, *130*, 853–864; c) Giner, X.; Nájera, C. *Org. Lett.* **2008**, *10*, 2919–2922;

11 a) Zhang, J.; Yang, C.-G.; He, C. *J. Am. Chem. Soc.* **2006**, *128*, 1798–1799; b) Liu, X.-Y.; Li, C.-H.; Che, C.-M. *Org. Lett.* **2006**, *8*, 2707–2710; c) Giner, X.; Nájera, C.; Kovács, G.; Lledós, A.; Ujaque, G. *Adv. Synth. Catal.* **2011**, *353*, 3451–3466; d) Timmerman, J. C.; Widenhoefer, R. A. *Adv. Synth. Catal.* **2015**, *357*, 3703–3706; e) Timmerman, J. C.; Robertson, B. D.; Widenhoefer, R. A. *Angew. Chem. Int. Ed.* **2015**, *54*, 2251–2254; f) Wang, C.; Ren, X.-R.; Qi, C.-Z.; Yu, H.-Z. *J. Org. Chem.* **2016**, *81*, 7326–7335; g) Couce-Rios, A.; Lledós, A.; Fernández, I.; Ujaque, G.; *ACS Catal.* **2019**, *9*, 848–858.

12 Zhang, Z.; Lee, S. D.; Widenhoefer, R. A. *J. Am. Chem. Soc.* **2009**, *131*, 5372–5373.

13 a) Dias, H. V. R.; Fianchini, M.; Cundari, T. R.; Campana, C. F. *Angew. Chem Int. Ed.* **2008**, *47*, 556–559; b) Schmidbaur, H.; Schier, A. *Organometallics* **2010**, *29*, 2–23; c) Cinellu, M. A. *in Modern Gold Catalyzed Synthesis*, Wiley-VCH, Weinheim, **2012**, 175–179; d) Brooner, R. E. M.; Widenhoefer, R. A. *Angew. Chem. Int. Ed.* **2013**, *52*, 11714–11724; e) Jones, A. C. *Top. Curr. Chem.* **2015**, *357*, 133–166; f) Navarro, M.; Bourissou, D. *Adv. Organomet. Chem.* **2021**, *76*, 101–144.

14 a) Zuccaccia, D.; Belpassi, L.; Tarantelli, F.; Machhioni, A. *J. Am. Chem. Soc.* **2009**, *131*, 3170–3171; b) de Frémont, P:, Marion, N.; Nolan, S. P. *J. Organomet. Chem.* **2009**, *694*, 551–560; c) Brown, T. J.; Dickens, M. G.; Widenhoefer, R. A. *Chem. Commun.* **2009**, 6451–6453; d)

Hooper, T. N.; Green, M.; McGrady, J. E.; Patel, J. R.; Russell, C. A. *Chem. Commun.* **2009**, 3877–3879; e) Moltoch, P.; Blahut, J.; Cisarova, I.; Roithová, J. *J. Organomet. Chem.* **2017**, *848*, 114–117; f) Griebel C.; Hodges, D.; Yager, B. R.; Liu, F. L.; Zhow, W.; Makaravage, K. J.; Zhu, Y.; Norman, S. G.; Lan, R.; Day, C. S.; Jones, A. C. *Organometallics* **2020**, *39*, 2665–2671.

15 a) Cinellu, M. A.; Minghetti, G.; Stoccoro, S.; Zucca, A.; Manassero, M. *Chem. Commun.* **2004**, 1618–1619; b) Cinellu, M. A.; Minghetti, G.; Cocco, F.; Stoccoro, S.; Zucca, A.; Manassero, M.; Arca, M. *Dalton Trans.* **2006**, 5703–5716; c) Flores, J. A.; Dias, H. V. R. *Inorg. Chem.* **2008**, *47*, 4448–4450; d) Dias, H. V. R.; Wu, J.; *Organometallics* **2012**, *31*, 1511–1517; e) Klimovica, K.; Krischbaum, K.; Daugulis, O. *Organometallics* **2016**, *35*, 2938–2943; f) Navarro, M.; Toledo, A.; Joost, M.; Amgounne, A.; Mallet-Ladeira, S.; Bourissou D. *Chem. Commun.* **2019**, *55*, 7974–7977; g) Navarro, M.; Toledo, A.; Mallet-Ladeira, S.; Sosa-Carrizo, E. D.; Miqueu, K.; Bourissou, D. *Chem. Sci.* **2020**, *11*, 2750–2758.

16 a) Dias, H. V. R.; Wu, J. *Angew. Chem. Int. Ed.* **2007**, *46*, 7814–7816; b) Ridlen, S. G.; Wu, J.; Kulkarni, N. V.; Dias, H. V. R. *Eur. J. Inorg. Chem.* **2016**, 2573–2580; c) Harper. M. J.; Arthur, C. J.; Crosby, J.; Emmet, E. J.; Falconer, R. L.; Fensham-Smith, A. J.; Gates, P. J.; Leman, T.; McGrady, J. E.; Bower, J.; Russell, C. A. *J. Am. Chem. Soc.* **2018**, *140*, 4440–4445; d) Yang, Y.; Antoni, P.; Zimmer, M.; Sekine, K.; Mulks, F. F.; Hu, L.; Zhang, L.; Rudolph, M.; Rominger, F.; Hashmi, A. S. K. *Angew. Chem. Int. Ed.* **2019**, *58*, 5129–5133; e) Wu, J.; Noonikara-Poyil, A.; Muñoz-Castro, A.; Dias, H. V. R. *Chem. Commun.* **2021**, *57*, 978–981.

17 Lang, S. M.; Bernhardt, T. M.; Barnett, R. N.; Landman, U. *Angew. Chem. Int. Ed.* **2010**, *49*, 980–983; b) Lang, S. M.; Bernhardt, T. M.; Bakker, M.; Yoon, B.; Landman, U. *J. Phys.: Condens. Matter.* **2018**, *30*, 504001; c) Metz, R. B.; Altinay, G.; Kostko, O.; Ahmed, M. *J. Phys, Chem. A.* **2019**, *123*, 2194–2202.

18 Keller, J.; Schlierf, C.; Nolte, P.; Straub, B. F. *Synthesis* **2006**, *2*, 354–365.

19 Navarro, M.; Miranda-Pizarro, J.; Moreno, J. J. Navarro-Gilabart, C.; Fernández, I.; Campos J. *Chem. Commun.* **2021**, *57*, 9280–9283.

20 a) Moreno, J. J.; Espada, M. F.; Campos, J.; López-Serrano, J.; Macgregor, S. A.; Carmona, E. *J. Am. Chem. Soc.* **2019**, *141*, 2205–2210; b) Ortega-Moreno, L.; Peloso, R.; López-Serrano, J.; Iglesias-Sigüenza, J.; Maya, C.; Carmona, E. *Angew. Chem. Int. Ed.* **2017**, *56*, 2772–2775; c) J. Organomet. Chem. 2019, 896, 120.

21 Espada, M. F.; Campos, J.; López-Serrano, J.; Poveda, M. L.; Carmona, E. *Angew. Chem. Int. Ed.* **2015**, *54*, 15379–15384.

22 Miranda-Pizarro, J.; Luo, Z.; Moreno, J. J.; Dickie, D. A.; Campos J.; Gunnoe, B. *J. Am. Chem. Soc.* **2021**, *143*, 2509–2522.

23 a) Campos, J. *J. Am. Chem. Soc.* **2017**, *139*, 2944–2947; b) Hidalgo, N.; Moreno, J. J.; Pérez-Jiménez, M.; Maya, C.; López-Serrano, J.; Campos, J. *Chem. Eur. J.* **2020**, *26*, 5982–5993; c) Hidalgo, N.; Moreno, J. J.; Pérez-Jiménez, M.; Maya, C.; López-Serrano, J.; Campos, J.

Organometallics **2020**, *39*, 2534–2544. d) Alférez, M. G.; Moreno, J. J.; Hidalgo, N.; Campos, J. *Angew. Chem. Int. Ed.* **2020**, *59*, 20863–20867.

24 Marín, M.; Moreno, J. J.; Navarro-Gilabert, C.; Álvarez, E.; Maya, C.; Peloso, R.; Nicasio, M. A.; Carmona, E. *Chem. Eur. J.* **2019**, *25*, 260–272.

25 Clavier, H.; Nolan, S. P. *Chem. Commun.* **2010**, *46*, 841–861.

26 Nes, G. J. H.; Vos, A. *Acta Crystallogr B.* **1979**, *B35*, 2593–2601.

27 Bayler, A.; Bowmaker, G. A.; Schmidbaur, H. *Inorg. Chem.* **1996**, *35*, 5959–5960.

28 Zhdanko, A.; Ströbele, M.; Maier, M. E. *Chem. Eur. J.* **2012**, *18*, 14732–14744.

29 a) Li, Q.-S.; Wan, C.-Q.; Zou, R.-Y.; Xu, F.-B.; Song, H.-B.; Wan, X.-J.; Zhang, Z.-Z. *Inorg. Chem.* **2006**, *45*, 1888–1890; Xu, F.-B.; Li, Q.-S.; Wu, L.-Z.; Leng, X.-B.; Li, Z.-C.; Zeng, X.-S.; Chow, Y. L.; Zhang, Z.-Z. *Organometallics* **2003**, *22*, 633–640; c) Lavallo, V.; Frey, G. D.; Kousar, S.; Donnadieu, B.; Bertrand, G. *Proc. Natl. Acad. Sci.* **2007**, *104*, 13569–13573; d) Jiménez-Núñez, E.; Claverie, C. K.; Nieto-Oberhuber, C.; Echavarren, A. M. *Angew, Chem. Int. Ed.* **2006**, *45*, 5452–5455; e) Weber, S. G.; Rominger, F.; Straub, B. F. *Eur. J. Inorg. Chem.* **2012**, 2863–3867; f) Parvin, N.; Mishra, B.; George, A.; Neralkar, M.; Hossain, H.; Parameswaran, P.; Hotha, S.; Kahn, S. *Chem. Commun.* **2020**, *56*, 7625–7628.

30 a) Homs, A.; Escofet, I.; Echavarren. A. M. *Org. Lett.* **2013**, *15*, 5782–5785; b) Weber, D.; Gagné. M. R.; *Org. Lett.* **2009**, *11*, 4962–4965

31 Calculations were performed with the Gaussian 09 program employing the hybrid functional PBE0. Geometry optimizations were carried out without geometry constraints and included solvent (dichloromethane) and dispersion effects (Grimme's D3 parameter set). The Goodvibes program was used to implement concentration, temperature and Truhlar's quasiharmonic free energy corrections.

32 The reaction coordinate was thoroughly mapped by means of relaxed potential energy scans, which confirmed its barrierless nature.

33 Uson, A.; Laguna, M.; Briggs, D. A.; Murray, H. H.; Fackler, J. P. *Inorg. Chem.* **2007**, *26*, 85–91.